Laser-Engraved Graphene for Flexible and Wearable Electronics

Minqiang Wang, Yiran Yang, Wei Gao[*]

Andrew and Peggy Cherng Department of Medical Engineering, California Institute of Technology, Pasadena, California, 91125, USA.

[*]Correspondence: weigao@caltech.edu.

Abstract

Laser-engraved graphene (LEG) has been increasingly applied in flexible electronics over the past decade owing to its unique physical and chemical properties, and has shown great promise in energy controls, chemical and physical sensing, and telemedicine. In-situ laser engraving has empowered graphene with more versatilities such as miniaturized patterning, tunable compositions, controllable morphologies, and environmental friendliness. In this review, the technological advances of the LEG from syntheses to applications in flexible and wearable electronic devices are summarized. Specifically, the use of the LEG in designing next-generation nanogenerators, batteries, supercapacitors, physical sensors, gas sensors, biosensors, and wearable/telemedicine systems is discussed. An outlook related to the LEG-based flexible electronics and key technological bottlenecks are identified.

The Emergence of Graphene in Flexible Electronics

Graphene has been broadly used in the development of flexible electronic devices and systems, thanks to its high theoretical specific surface area, mobility, flexibility, mechanical strength, conductivity, and biocompatibility [1-6]. The fabrication of graphene is commonly achieved by chemical vapor deposition, mechanical exfoliation, and wet chemical reduction of graphene oxide (GO) [7-9]. Although conventional processing techniques, such as screen-printing, roll-to-roll printing, and inkjet printing, have been used to fabricate the graphene-based devices [10-12], in most cases, re-stacking of the graphene sheets in the presence of additives hindered their performance [13, 14]. An important frontier lies in the large-scale low-cost production of high performance and versatile graphene-based electronics for wide-range applications of graphene in consumer devices, and laser-engraved graphene (LEG) has shown great potentials to this end. This article provides an overview of recent advances on LEG and LEG-based flexible electronics

as illustrated in Figure 1. The in-situ synthesis and characterization of LEG from precursor substrate are summarized along with the laser reduction of GO. Subsequently, LEG-enabled functionalities toward flexible electronics, including energy control, chemical and physical sensing, and system-level of telemedicine are reviewed in detail. Challenges and outlook are discussed towards the applications of LEG for personalized healthcare.

Laser-Engraved Graphene

Laser processing technologies permit scalable patterning of graphene on various substrates, mostly either via laser-induced direct carbonization of polymeric substrates (e.g., PI, polyethyleneimine) or laser-induced reduction of GO. Considering that laser engraving plays a crucial role in both strategies for graphene formation and patterning, we categorize all resulted graphene structures as LEG in this review. Ultraviolet (UV) laser ablation was initially used to pattern carbonized structure on polyimide (PI) film in the 1990s [15]. In the 2010s, it was found that commercially available CO_2 laser cutters could be used to directly engrave and pattern porous graphene on various synthetic and natural carbon precursor (e.g., PI) substrates under ambient conditions [16] without generating hazardous wastes [17]. Since then, LEG has shown tremendous potentials in flexible electronics applications as it has unique electrical and chemical properties and allows rapid customizable prototyping at a large scale and at a low cost (Table 1) [18-20].

Direct Laser Engraving

Direct graphene patterning can be achieved with lasers of various wavelengths, spanning from UV to infrared (IR) ranges (Figure 2A) [33]. When the laser beam reaches the precursor of graphene (i.e. polyimide), graphene forms in a photochemical and/or photothermal process. The photochemical reaction usually appears when a short-wavelength (i.e., UV or blue) laser source is used, as its high photon energy absorbed can directly break chemical bonds and form a dense graphene structure (Figure 2B-D) [33, 34]; The photothermal reaction could become predominant when a longer-wavelength (i.e., IR) laser source is used, as the absorbed laser energy is converted to local heat and thus leads to a high localized temperature (>2500 ℃) [16]. It should be noticed that multiple laser parameters (e.g., wavelength [22, 35, 36], power [37], pulse width [38], and scanning speed) play a key role in the final graphene structure formation and

should be considered concurrently during graphene fabrication. When engraving the PI with a 10.6 μm CO_2 laser cutter, chemical bonds in the PI network are broken and thermal reorganization of the carbon atoms occurs, resulting in sheets of graphene structures (Figure 2E-G) [30, 33]. It has been shown that such LEG flakes are full of defects expanding a hexagon lattice with two pentagons and one heptagon, which could lead to a porous structure [39]. With custom laser settings, different morphologies of the graphene structure can be directly patterned on polyimide, ranging from isotropic pores, cellular networks and nanofibers [37].

Although laser engraving remains a 2D-patterning process, various strategies have been developed to utilize laser engraving to achieve 3D graphene foam of various structures. Laminated object manufacturing was utilized to stack multiple layers of PI-based LEG together and the resulted cubed graphene foam was further carved to the desired shape with fiber laser milling [40]. Furthermore, layer-by-layer CO_2 laser sintering was performed on Ni-sucrose powder and enabled free-standing graphene foam structures with high porosity and electrical conductivity [41].

Laser Reduction of GO

GO, prepared via chemical exfoliation of graphite, can be converted to reduced graphene oxide (rGO) with defined patterns directly by laser radiation and provide feasible strategies for graphene-based electronics. It has rich oxygen-containing groups (OCGs) on the graphene skeleton and has a high photon absorption thanks to its narrowband structures. These OCGs can be cut down through photochemical and photothermal processes easily, even with a weak photon energy laser (Fig. 2H) [42]. Under laser thermal reduction, GO undergoes a disproportionation reaction to yield r-GO, accompanied by the evolution of the carbonaceous gases. Huang and coworkers described the detailed chemical reactions involved during the thermal reduction of GO [43]. The GO nano-flakes can be easily deployed onto various substrates and then rGO can be directly patterned on the substrate. The rGO microcircuits on a GO film were fabricated via a mask-free manner with 800 nm femtosecond laser reduction; the in-plane rGO/GO/rGO nano-configuration is illustrated in Figure 2I [44]. The degree of reduction and the conductivity of the rGO obtained under different laser power settings were investigated via current-sensing atomic force microscopy (CSAFM). As shown in Figure 2J, while the GO film remains insulated, the

rGO pattern reduced with an 8-mW laser becomes conductive [45]. Laser reduction also results in a 3D hierarchical structure which contributes to the high conductivity and anisotropy of the laser-engraved rGO [46, 47].

LEG-based Energy Control Devices

Flexible energy control devices are promising solutions for efficient energy harvesting and storage. Laser processing substantially simplifies the manufacturing and integration of graphene structures in flexible energy control. A wide range of LEG-based flexible energy control devices are developed recently and summarized in this section.

LEG-based Energy Harvesting Devices

Triboelectric nanogenerator (TENG) is a highly attractive energy harvesting approach capable of harvesting mechanical energy and converting it into electricity [48, 49] . A flexible TENG-based on a MXene-polydimethylsiloxane composite film and an LEG electrode was developed (Figure 3A); this TENG, used as a writing board, produces voltage signal based on the contact electrification as well as electrostatic induction between two electrodes [50]. LEG was also utilized as high-efficiency TENG electrodes which produced a significantly higher electrical output compared to adhesive aluminum electrodes [51].

Direct laser patterned rGO was successfully applied in the flexible organic photovoltaics (OPVs) devices (Figure 3B), which displayed a high power conversion efficiency for flexible OPVs devices [52]. The optical and electrical properties of the rGO micromesh were tuned by controlling the periodicity, irradiation time, and neck width of the mesh and the device possesses unique properties such as excellent flexibility, transparency, and conductivity.

In addition to the TENG and the OPVs, LEG has been employed in the development of integrated flexible biofuel cells, as demonstrated in Figure 3C. The LEG-based bioanode and biocathode were modified with glucose dehydrogenase (GDH) and bilirubin oxidase (BOD), respectively. Owing to the high conductivity and electrochemical performance of the LEG, the constructed biofuel cell produced a maximum power density to 27 ±1.7 μW cm^{-2} at the open circuit voltage of 0.45 ± 0.03 V. In addition, the device displayed great mechanical robustness and lifetime [53].

LEG-based Energy Storage Devices

LEG has been used in the development of flexible energy storage devices such as rechargeable batteries [54-57]. With an ultrahigh theoretical energy density of 1218 Wh kg^{-1}, Zn-air battery is a promising alternative energy storage device, but there is a pressing need for an inexpensive and efficient cathode [54, 55]. Integration of the LEG with different nanomaterials can enrich its functionality and offer an attractive approach for preparing high-performance low-cost battery cathode. As shown in Figure 3D, a ternary metal oxide/LEG hybrid dual oxygen reduction reaction/oxygen evolution reaction catalyst was directly fabricated using CO_2 laser by engraving the precursor (Co, Ni, and Fe ions)-loaded LEG [56]. After assembly of the optimized catalyst cathode with a zinc plate as the anode, a flexible Zn-air battery was prepared and displayed a peak discharge power density of 98.9 mW cm^{-2} and an energy density of 842 Wh kg^{-1}. The introduction of the LEG significantly increased the specific surface area and porosity of the catalyst, thereby substantially increasing the catalytic active sites. With a significant reduction of the nucleation barrier of lithium ions, the LEG-based composite material was also applied to improve the coulomb efficiency and capacity degradation of lithium-metal anode [58].

Supercapacitors are electrical energy storage devices based on the mechanism of electrical double layer capacitance, and the typical layout of supercapacitors includes either planar or thin film interdigitated architectures [59]. An in-plane interdigital configuration micro-supercapacitor electrode was patterned directly with laser on GO-coated substrates [60]. Direct laser reduction of GO to rGO on a standard LightScribe DVD optical drive was performed to fabricate in-plane electrodes with excellent electrical conductivity (1738 S m^{-1}) and large surface area (1520 m^2 g^{-1}) [61]. The electrodes can thus be used to fabricate an all-solid-state flexible supercapacitor, which exhibits excellent energy density and stability after 1000 cycles of bending tests (Figure 3E). Scalable fabrication of the LEG-micro-supercapacitors on flexible substrate leads to a very high power density of ~200 W cm^{-3} [24]. Although GO can be developed as a supercapacitor devices with great performance, the coating of the GO increased the fabrication complexity. The LEG electrodes with 3D porous structure dramatically enlarged the surface area which increases the specific capacitance. With these benefits, LEG has thereby been widely used to improve the performance of the supercapacitors [16, 62].

LEG-based Physical Sensors and Gas Sensors

Owing to the unique electronic properties, LEG could serve as a great candidate for monitoring physical parameters (e.g., temperature and strain) and gas molecules by detecting the changes of the LEG's electrical properties (e.g., resistance and impendence). In this section, we summarize the mechanism of the LEG-based physical and gas sensing toward physiological monitoring of vital signs.

Temperature and Strain Sensors

The unique 3D LEG structures with tuned laser parameters can be used for designing temperature or strain sensors [22, 32, 63-65] . As illustrated in Figure 4A, B, vector mode laser engraving can be used to fabricate micro-structures sensitive to temperature and strain. By controlling the sensors layout design and laser settings, the LEG temperature sensor can be designed to be less susceptible to strain variations while the strain sensor can be optimized to achieve the highest strain response [30]. Increased temperature can lead to an increase in LEG conductivity due to the enhanced electron-phonon scattering and the electron thermal velocity of electrons in the sandwiched layer, rendering its negative temperature coefficients (Figure 4A). The LEG-based strain sensors are based on the piezoresistive effect with its ultra-porous structure (Figure 4B); when an external strain is applied, the compressed 3D porous structure of the strain sensor results in a decrease in resistance, which could be further used for accurate monitoring of respiration rate and heart rate.

Gas and Humidity Sensors

Laser-treated rGO is attracting more research interests in gas sensing [66]. The adsorption and desorption of gas molecules on the rGO surface change its resistance. An all-graphene flexible nitrogen dioxide (NO_2) sensor was developed and was used for reversible NO_2 detection via the change in sheet resistance [67]. Although graphene has excellent sensing properties toward polar molecules, it is insensitive to most non-polar molecules such as H_2. As demonstrated in Figure 4C, via in-situ laser cutting, noble metal atoms sensitive to H_2 molecules are modified onto the surface of graphene, realizing an artificial nose for highly sensitive H_2 detection [68]. In addition to gas molecules, rGO also enables the sensing of humidity due to the strong interaction between OCGs and water molecules. With tuned laser engraving, rGO with different OCGs content and different conductivity can be obtained, enabling a high sensitivity in detecting environmental

humidity [46]. A flexible humidity sensor with LEG interdigital electrodes and a humidity-sensitive GO film was engraved on a flexible PI substrate for capacitive sensing-based human respiration sensing with high sensitivity, low hysteresis, and long-term stability (Figure 4D) [69].

LEG-based Vital Sign Monitors

Wearable and flexible physiological monitors are able to collect the key vital signs continuously and play a crucial role in personalized healthcare [70]. An LEG artificial throat was fabricated through a photochemical process using a 450 nm laser source (Figure 4E). Various throat vibrations produced by coughs, hums, screams, swallowing and nods could be monitored by measuring the resulted resistance change of the wearable LEG device [34]. In addition, the integration of electrical properties of black phosphorus and LEG demonstrated a paradigm for dual-model temperature and strain sensing platform to modulate the e-skin's sensing functionality (Figure 4F) [71]. The excellent physical properties of the LEG and the LEG composites render excellent performance in detecting many other health-related physical signals, including passive pressure, diastolic and systolic blood pressure, electrocardiogram (ECG), and arterial pulse waveforms [72, 73].

LEG-based Biosensors

Biosensors, relying on chemical reactions or biorecognition for target molecular detection, provide an essential solution to assess human health at molecular levels. LEG is a new promising candidate in electrochemical biosensors due to the attractive electrochemical properties such as the large surface area, the excellent stability, and abundant catalytic active sites which improve the electron transfer kinetics significantly and thereby enable the sensitive detection of biomarkers in biofluids.

Direct Molecular Detection on the LEG

Benefiting from the rich catalytic active sites induced by the laser engraving process, highly active LEG can directly differentiate and quantify electroactive analytes that have intrinsically distinct oxidation potentials. For example, a flexible LEG chemical sensor for continuous uric acid (UA) and tyrosine (Tyr) monitoring was developed (Figure 5A) [30]. Other electroactive small molecules such as dopamine (DA), epinephrine (EP), norepinephrine (NE), hydrazine, and

sodium sulfate could also be detected this way [74-76]. Functionalization of LEG with metallic nanoparticles endows pristine LEG with an increased conductivity and improved sensitivity [77-80]. In addition to direct detection of electroactive molecules, functionalization of LEG with ion selective membranes realizes real-time monitoring of a variety of ions (e.g., K^+, NH_4^+, Ca^{2+}) via potentiometry [38, 81, 82]. With the modification of polyaniline, a highly stretchable LEG-based potentiometric pH sensor was developed for point-of-care applications [81]. Alternatively, sensitive detection of heavy metal ions was achieved on the LEG with stripping voltammetry that involved deposition of the target metal phase onto the electrode followed by the selective oxidation of the deposited metal film (Figure 5B) [83].

LEG-based Bioaffinity Sensors

In contrast to the direct chemical sensing on the LEG, LEG-based bioaffinity sensors are established by modifying the LEG surface with "bioreceptors" such as antibodies, molecularly imprinted polymers (MIPs), and aptamers [84]. The synergistic combination of the conductive LEG and recognition elements (bioreceptors) renders an extraordinary sensing selectivity and sensitivity. As schematically illustrated in Figure 5C, an LEG-based competitive electrochemical immunosensor was developed to monitor the diurnal dynamics of cortisol and stress response in biofluids (serum, saliva, and sweat) [31]. LEG-based label-free electrochemical immunosensors can also be designed to detect *salmonella enterica* without sample preconcentration [85]. Instead of natural antibodies, MIPs have been deemed as biomimetic "artificial receptors" and display excellent binding selectivity to target molecules. The modifications of MIPs on two conductive LEG working electrodes enabled the highly sensitive detection of amoxicillin (AMOX) and AA with great sensitivities and selectivities [86] (Figure 5D). Aptamer, another alternative affinity bioreceptor, was used to functionalize the LEG electrodes for thrombin detection in a redox system; the sensor displayed picomolar sensitivity in the complex matrix of serum (Figure 5E) [87].

LEG for Wearable and Telemedicine Applications

The attractive physical, chemical, and mechanical properties of the LEG provide feasible means for large-scale low-cost fabrication of wearable and telemedicine sensor patches towards personalized healthcare applications. Transferring or printing the LEG fabricated from the PI

substrate to a more flexible, stretchable, and gas-permeable substrate allows conformal contact with the skin, enabling high-performance wearable sensing with attractive mechanical resiliency for vital sign monitoring [32, 88]. A soft and gas-permeable device was fabricated integrating laser-patterned porous graphene on sugar-templated silicone elastomer sponges (Figure 6A), and the resulted device showed excellent performance in on-body monitoring of electrophysiological signals, temperature, and hydration [32]. Considering that continuous sweat analysis could provide insightful information about an individual's health state at molecular levels [29, 89, 90], an all-laser-engraved multimodal lab-on-skin was developed which consisted of the LEG-based physical sensors for vital sign monitoring (e.g., temperature, heart rate, and respiration), the LEG-based chemical sensor for monitoring of trace-level sweat metabolites and nutrients (e.g., UA and Tyr), and a microfluidic module for efficient sweat sampling (Figure 6B) [30]. This wireless wearable platform was successfully evaluated in a pilot study involving both healthy subjects and gout patients toward non-invasive gout management through real-time, continuous monitoring of sweat UA (Figure 6B) [30]. To combat the COVID-19 pandemic, a fully integrated point-of-care LEG-based multiplex telemedicine platform – SARS-CoV-2 RapidPlex – was developed for rapid COVID-19 diagnosis and management (Figure 6C). It could simultaneously and quantitatively analyze the virus antigen, virus antibodies, and C-reactive protein in saliva and blood samples from COVID-19 patients, providing information on current infection, infection severity, and immune response [29].

Concluding Remarks

Recent progress in laser-engraved graphene sensors has revealed the versatile use of graphene for energy control, physical sensing, direct chemical sensing, and affinity-based biosensing. Compared to conventional graphene fabrication techniques, the laser-engraving process allows simple, mass-producible, and inexpensive graphene patterning in ambient conditions. Various LEG features including porosity, composition, impedance, and morphology can be tuned upon different laser parameters, rendering possibilities for diverse flexible on-skin electronic devices. The high biocompatibility, gas-permeability, and antibacterial properties of LEG are also beneficial to its bioelectronics and wearable applications.

Despite the great promise, there are critical challenges to be resolved to realize the full potential

of the LEG, such as relatively low mobility (compared to vacuum-processed graphene [91]), the mechanical stability of LEG on the flexible substrate, poor stretchability compared to elastomers, and the durability for long-term on-skin use. The electrical and mechanical properties may be potentially improved with strategic polymeric coating or optimization of the laser engraving parameters. In situ and ex-situ modification on LEG could further enhance its properties such as electrical conductivity and specificity in both physical and chemical sensing. Highly stretchable LEG-based electronic devices can be potentially achieved through transfer printing of the patterned LEG onto a soft elastomer substrate. Moreover, although current source materials for direct laser-engraved graphene are mostly based on PI and polyethyleneimine, new choices materials are being explored, such as lignin-containing wood [92], sulfonated poly(ether ketone) [93], and phenolic resin [23], which could also potentially shed light on resolving some of the challenges aforementioned. Nonetheless, the diversity of use of LEG has resulted in fruitful applications and with future research endeavors, LEG-based flexible electronics may become commonplace products in future wearables.

Acknowledgments

This project was supported by the Translational Research Institute for Space Health through NASA NNX16AO69A, Office of Naval Research Award N00014-21-1-2483, High Impact Pilot Research Award T31IP1666 and grant R01RG3746 from the Tobacco-Related Disease Research Program.

Declaration of interests

No interests are declared.

Glossary

Bioaffinity sensor: A biosensing approach that utilize a bioreceptor for specific recognition of the target analyte.

Chemical vapor deposition: A vacuum deposition method used to produce high quality, high-performance, solid materials.

Mechanical exfoliation: A top-down approach that requires mechanical energy in order to exfoliate graphite.

Triboelectric nanogenerators: Devices that convert mechanical energy to electricity using the triboelectric effect.

Wet chemical reduction of graphene oxide: A protocol that utilizes chemical reactions in the solution phase to prepare graphene from a form of graphene oxide.

Telemedicine: A practice of medicine using technology to deliver care at a distance and allowing remote patient and clinician contact, care, advice, intervention, and monitoring.

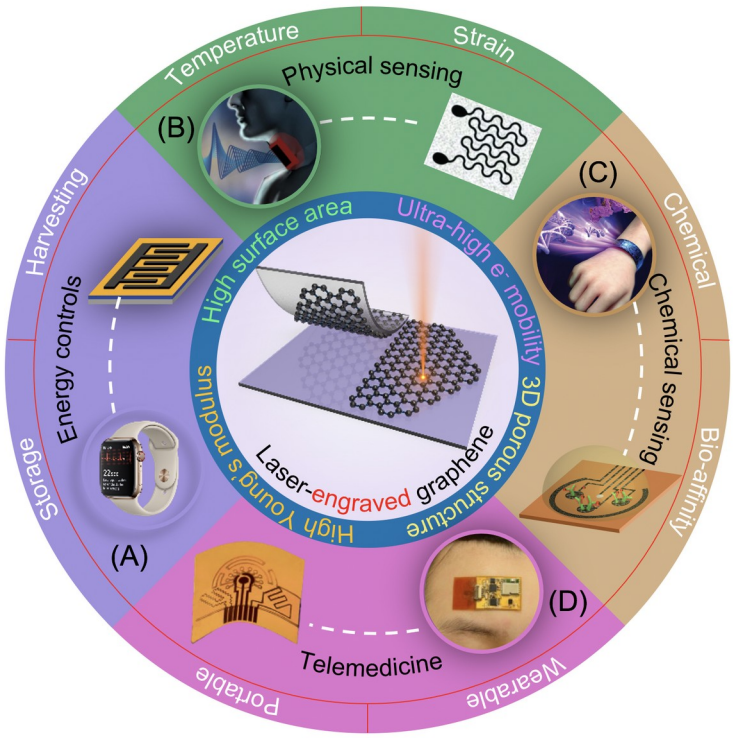

Figure 1. An overview of the LEG-based flexible and wearable electronic devices. (A) LEG-based energy control. Adapted with permission from [24]. (B) LEG-based physical sensing. Adapted with permission from [32, 34]. (C) LEG-based chemical sensing. Adapted with permission from [31, 84] . (D) LEG-based telemedicine. Adapted with permission from [30].

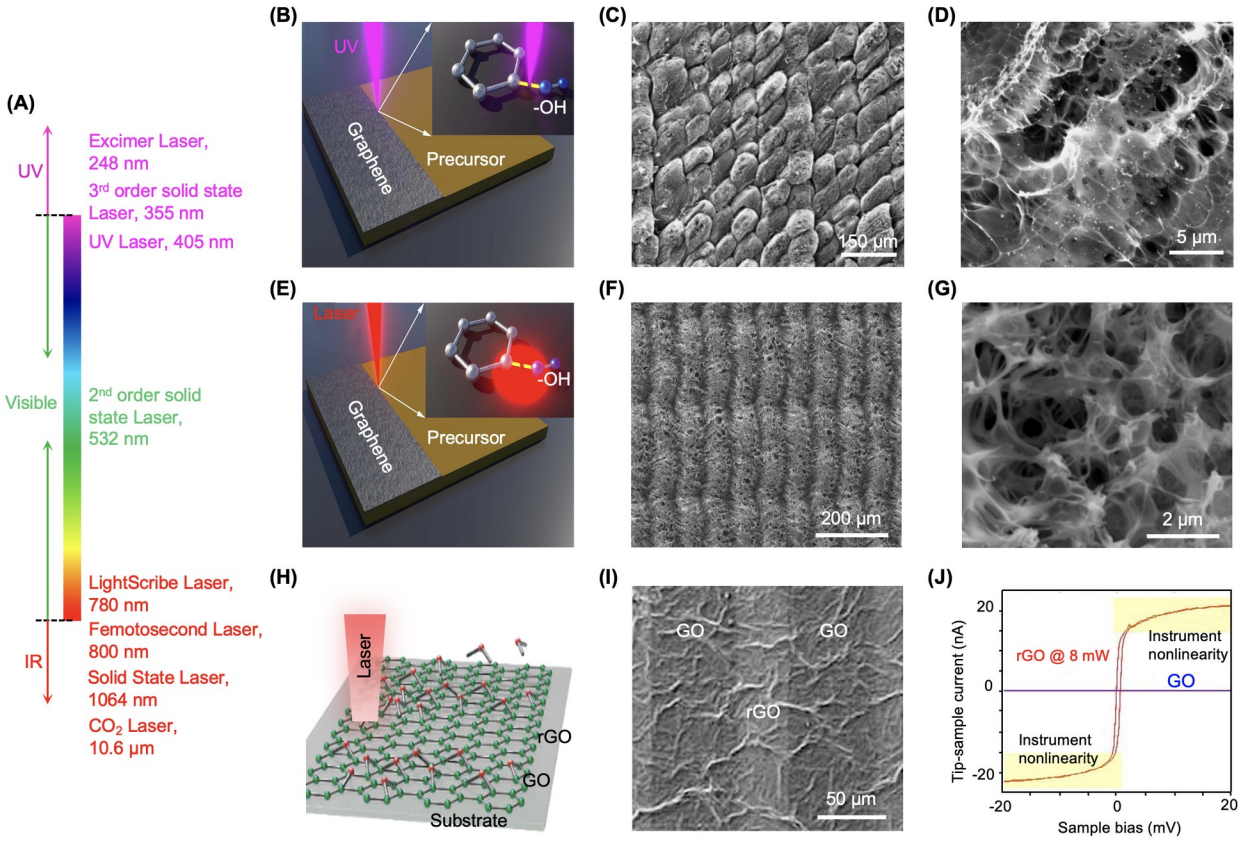

Figure 2. Fabrication and characterization of the LEG. (A) Laser sources used for graphene engraving. (B) Schematic of the photochemical process using UV as energy source. Adapted with permission from [33]. (C, D) SEM images of the LEG on PI produced by a 450 nm laser. Adapted with permission from [34]. (E) Schematic of the photothermal reorganization process of the LEG from precursor substrates. Adapted with permission from [33]. (F, G) SEM image of the LEG on PI produced by a CO_2 laser Adapted with permission from [30]. (H) Schematic illustration of the laser reduction of GO to rGO. (I) SEM image of the plane rGO/GO/rGO configuration on the GO film. Adapted with permission from [44]. (J) Current-sensing atomic force microscopy *I-V* curves of the rGO reduced with an 8-mW laser. Adapted with permission from [45].

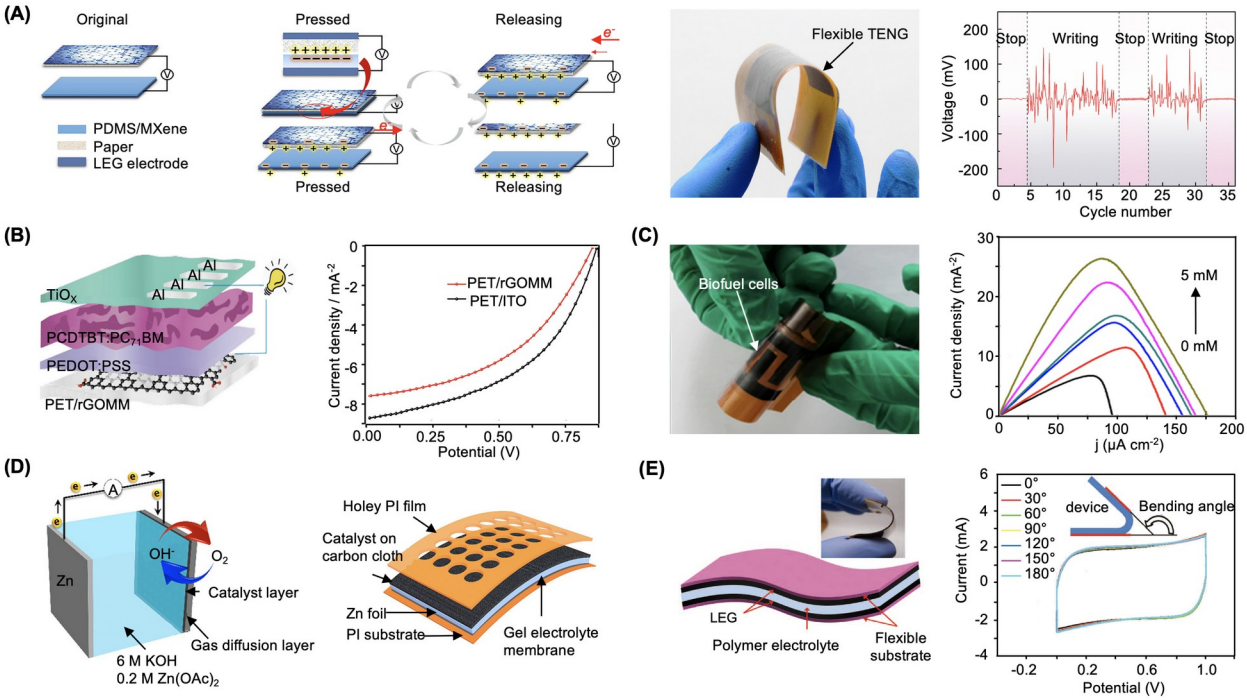
(A)
Original
Pressed
Releasing
PDMS/MXene
Paper
LEG electrode
Pressed
Releasing
Flexible TENG
Stop
Writing
Stop
Writing
Stop
Voltage (mV)
Cycle number
(B)
Al
TiOx
PCDTBT:PC71BM
PEDOT:PSS
PET/rGOMM
PET/rGOMM
PET/ITO
Current density / mA-2
Potential (V)
(C)
Biofuel cells
5 mM
0 mM
Current density (mA-2)
j (μA cm-2)
(D)
A
e
OH-
O2
Zn
Catalyst layer
Gas diffusion layer
6 M KOH
0.2 M Zn(OAc)2
Holey PI film
Catalyst on carbon cloth
Zn foil
PI substrate
Gel electrolyte membrane
(E)
LEG
Polymer electrolyte
Flexible substrate
0°
30°
60°
90°
120°
150°
180°
device
Bending angle
Current (mA)
Potential (V)

Figure 3. LEG for energy controls. (A) An LEG-based TENG writing tablet for writing motion monitoring. Adapted with permission from [50]. (B) A bulk-heterojunction flexible organic photovoltaic (BHJ OPV) device with the LEG as transparent conductive electrode. Adapted with permission from [52]. (C) An LEG-based enzymatic glucose biofuel cells. Adapted with permission from [53]. (D) A LEG-based rechargeable Zn-Air battery. Adapted with permission from [56]. (E) An all-solid-state LEG-based flexible electrochemical capacitor. Adapted with permission from [61].

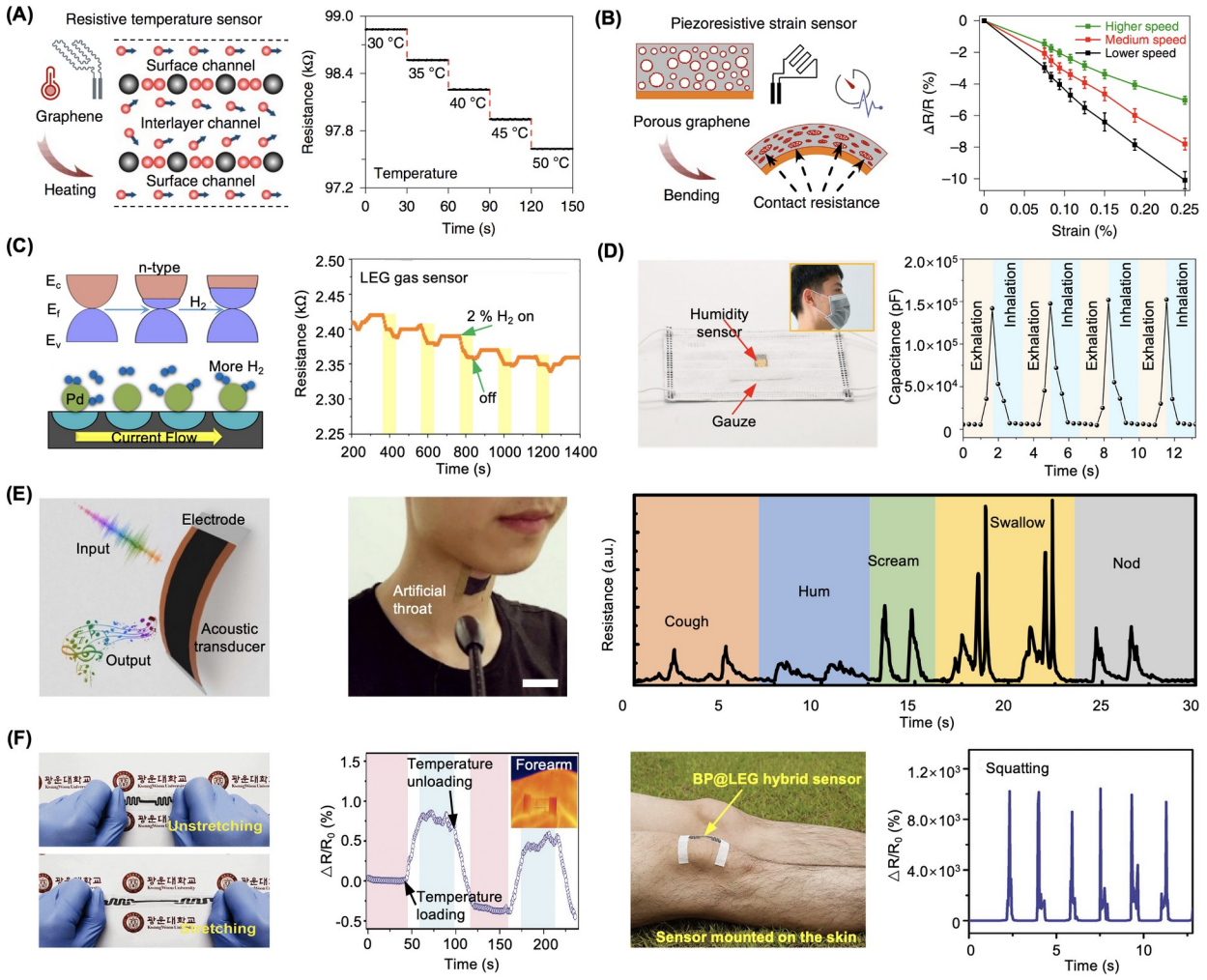

Figure 4. LEG-based physical sensors and gas sensors. (A) Mechanism and dynamic response of a LEG-based temperature sensor. (B) Mechanism and strain responses of LEG-based train sensors. Adapted with permission from [30]. (C) An LEG-based H_2 sensor. Adapted with permission from [68]. (D) An LEG-based humidity sensor for respiration monitoring. Adapted with permission from [69]. (E) An LEG-based artificial throat towards real-time throat vibration monitoring. Adapted with permission from [34]. (F) Black phosphorus@LEG heterostructure-based temperature-strain hybrid sensor. Adapted with permission from [71] .

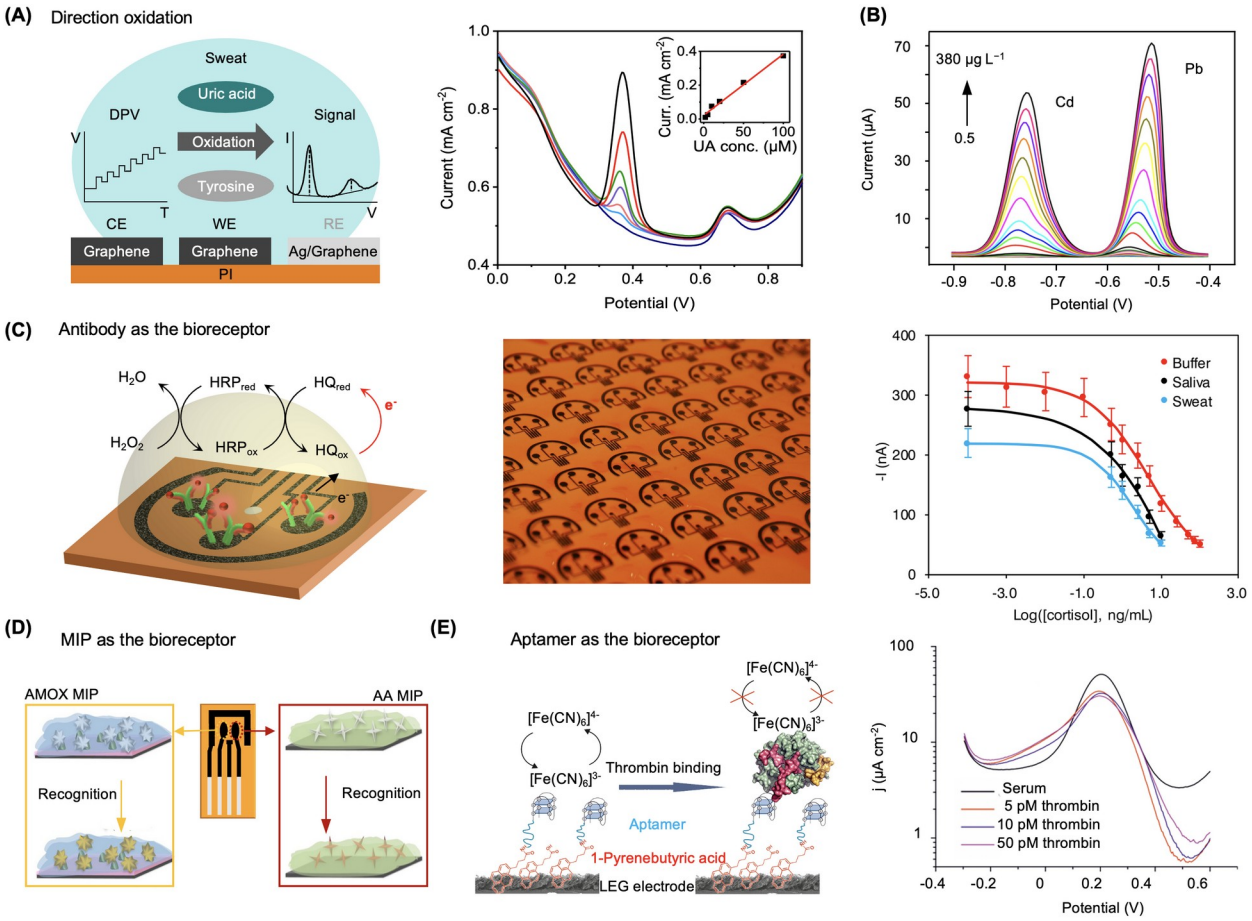

Figure 5. LEG-based biosensors. (A) An LEG-based biosensor for simultaneous UA and Tyr detection. Adapted with permission from [30]. (B) Dynamic responses of an LEG-based heavy metal sensor. Adapted with permission from [83]. (C) An LEG-based electrochemical immunosensor array for rapid sweat cortisol monitoring. Adapted with permission from [31]. (D) An LEG-based dual-MIP sensor for the detection of AA and AMOX. Adapted with permission from [86]. (E) An LEG-based aptamer sensor for electrochemical thrombin detection. Adapted with permission from [87].

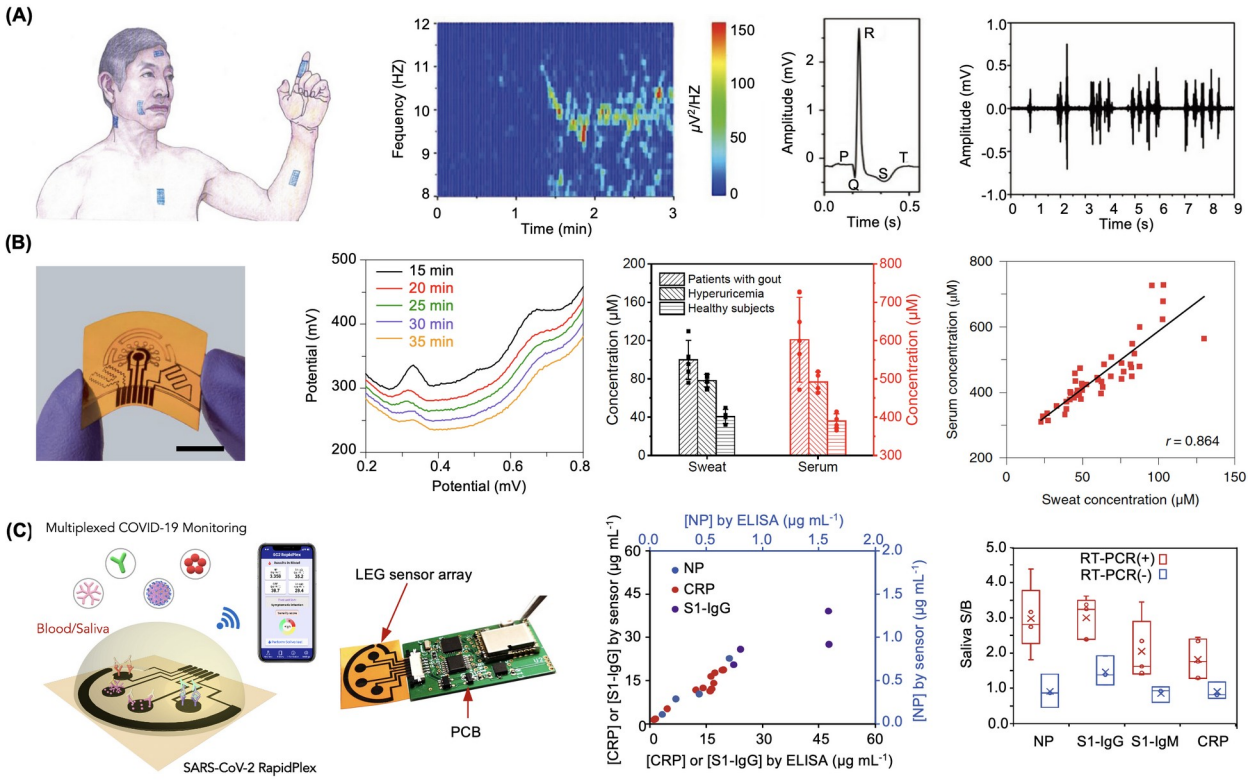

Figure 6. LEG for wearable and telemedicine applications. (A) The LEG-based multifunctional devices to monitor electrophysiological activities including alpha rhythm, ECG, and EMG. Adapted with permission from [32]. (B) A flexible all-laser-engraved multimodal wearable patch for the dynamic monitoring of sweat UA toward gout management. Adapted with permission from [30]. (C) A multiplexed telemedicine platform SARS-CoV-2 RapidPlex for rapid COVID-19 diagnosis and monitoring. Adapted with permission from [29].

Table 1. LEG prepared with different condition and their application.

Precursors	Laser source	Parameters (wavelength/pulse duration/intensity)	Applications	Ref.
Graphite oxide	KrF excimer laser	308 nm, 105 mJ cm^{-2}	Supercapacitors	[21]
PI	UV	355 nm, 1 μs, 300 mW	Strain sensing	[22]
Phenolic resin	Visible light	405 nm, 2 μs, 500 mW	Supercapacitors	[23]
GO film	LightScribe DVD optical drive	780 nm, 5 mW	Supercapacitors	[24]
GO	Femtosecond laser	800 nm, 120 fs, 16–60 nJ	Electronic circuits and memory cards	[25]
V_2O_5-GO film	Near IR laser	1064 nm, 10 μs	Supercapacitor	[26]
Metal-complex-containing polyethersulfone	CO_2 laser	10.6 μm, 40 W	Photoelectrochemical sensing	[27]
Cloth, paper, and food	CO_2 laser	10.6 and 9.3 μm, 75 and 50 W	Supercapacitors	[17]
Kevlar textile	CO_2 laser	10.6 μm, 5.5–8.0 W	Zn−air battery, ECG monitoring, NO_2 sensing	[28]
PI	CO_2 laser	10.6 μm, 14 μs, 2.4–5.4 W	Supercapacitors	[16]
PI	CO_2 laser	10.6 μm, 50 W	COVID-19 diagnosis	[29]
PI	CO_2 laser	10.6 μm, 50 W	Multi-module sweat analysis	[30]
PI	CO_2 laser	10.6 μm, 50 W	Sweat cortisol analysis	[31]
PI	CO_2 laser	10.6 μm, 14 μs, 30 W	EEG, ECG, and EMG monitoring	[32]

References

1. Geim, A. K. (2009) Graphene: status and prospects. *Science* 324, 1530–1534.

2. Han, T. -H. *et al.* (2017) Graphene-based flexible electronic devices. *Mater. Sci. Eng. R Rep.* 118, 1–43.

3. Kim, S. J. *et al.* (2015) Materials for flexible, stretchable electronics: graphene and 2D materials. *Annu. Rev. Mater. Res.* 45, 63–84.

4. Zhang, Z. *et al.* (2017) Rosin-enabled ultraclean and damage-free transfer of graphene for large-area flexible organic light-emitting diodes. *Nat. Commun.* 8, 14560.

5. You, R. *et al.* (2020) Laser fabrication of graphene-based flexible electronics. *Adv. Mater.* 32, e1901981.

6. Khan, U. *et al.* (2017) Graphene tribotronics for electronic skin and touch screen applications. *Adv. Mater.* 29, 1603544.

7. Chen, Z. *et al.* (2011) Three-dimensional flexible and conductive interconnected graphene networks grown by chemical vapour deposition. *Nat. Mater.* 10, 424–428.

8. Xu, Y. *et al.* (2010) Self-assembled graphene hydrogel via a one-step hydrothermal process. *ACS Nano* 4, 4324–4330.

9. Eigler, S. et al. (2013) Wet chemical synthesis of graphene. *Adv. Mater.* 25, 3583–3587.

10. Bae, S. *et al.* (2010) Roll-to-roll production of 30-inch graphene films for transparent electrodes. *Nat. Nanotech.* 5, 574.

11. Hyun, W. J. *et al.* (2015) High-resolution patterning of graphene by screen printing with a silicon stencil for highly flexible printed electronics. *Adv. Mater.* 27, 109–115.

12. Capasso, A. *et al.* (2015) Ink-jet printing of graphene for flexible electronics: an environmentally-friendly approach. *Solid State Commun*. 224, 53–63.

13. Zhang, Y. *et al.* (2012) Glass carbon electrode modified with horseradish peroxidase immobilized on partially reduced graphene oxide for detecting phenolic compounds. *J. Electroanal. Chem.* 681, 49–55.

14. Wang, F. *et al.* (2014) A simple, rapid and green method based on pulsed potentiostatic electrodeposition of reduced graphene oxide on glass carbon electrode for sensitive voltammetric detection of sophoridine. *Electrochim. Acta* 141, 82–88.

15. Srinivasan, R. *et al.* (1995) Chemical transformations of the polyimide Kapton brought about by ultraviolet laser radiation. *J. Appl. Phys.* 78, 4881–4887.

16. Lin, J. *et al.* (2014) Laser-induced porous graphene films from commercial polymers. *Nat. Commun.* 5, 5714.

17. Chyan, Y. *et al.* (2018) Laser-induced graphene by multiple lasing: toward electronics on cloth, paper, and food. *ACS Nano* 12, 2176–2183.

18. Ye, R. *et al.* (2018) Laser-induced graphene. *Acc. Chem. Res.* 51, 1609–1620.

19. Ye, R. *et al.* (2019) Laser-induced graphene: from discovery to translation. *Adv. Mater.* 31, 1803621.

20. Luong, D. X. *et al.* (2019) Laser-induced graphene composites as multifunctional surfaces. *ACS Nano* 13, 2579–2586.

21. Hosseini, S.M. et al. (2018) Excimer laser assisted very fast exfoliation and reduction of graphite oxide at room temperature under air ambient for Supercapacitors electrode. *Appl. Surf. Sci.* 427, 507-516.

22. Carvalho, A. F. *et al.* (2018) Laser-induced graphene strain sensors produced by ultraviolet irradiation of polyimide. *Adv. Funct. Mater.* 28, 1805271.

23. Zhang, Z. et al. (2018) Visible light laser-induced graphene from phenolic resin: a new approach for directly writing graphene-based electrochemical devices on various substrates. *Carbon* 127, 287–296.

24. El-Kady, M. F. and Kaner, R. B. (2013) Scalable fabrication of high-power graphene micro-supercapacitors for flexible and on-chip energy storage. *Nat. Commun.* 4, 1475.

25. Liang, J. et al. (2010) Toward all-carbon electronics: fabrication of graphene-based flexible electronic circuits and memory cards using maskless laser direct writing. *ACS Appl. Mater. Inter.* 2, 3310–3317.

26. Zhang, L.-F. et al. (2017) A laser irradiation synthesis of strongly-coupled VOx-reduced graphene oxide composites as enhanced performance supercapacitor electrodes. *Mater. Today Energy* 5, 222–229.

27. Ge, L. *et al.* (2019) Direct-laser-writing of metal sulfide-graphene nanocomposite photoelectrode toward sensitive photoelectrochemical sensing. *Adv. Funct. Mater.* 29, 1904000.

28. Wang, H. et al. (2020) Laser writing of janus graphene/kevlar textile for intelligent protective clothing. *ACS Nano* 14, 3219–3226.

29. Torrente-Rodríguez, R. M. *et al*. (2020) SARS-CoV-2 RapidPlex: a graphene-based multiplexed telemedicine platform for rapid and low-cost COVID-19 diagnosis and monitoring. *Matter* 3, 1981–1998.

30. Yang, Y. *et al.* (2020) A laser-engraved wearable sensor for sensitive detection of uric acid and tyrosine in sweat. *Nat. Biotech.* 38, 217–224.

31. Torrente-Rodríguez, R. M. *et al.* (2020) Investigation of cortisol dynamics in human sweat using a graphene-based wireless mHealth system. *Matter* 2, 921–937.

32. Sun, B. *et al.* (2018) Gas-permeable, multifunctional on-skin electronics based on laser-induced porous graphene and sugar-templated elastomer sponges. *Adv. Mater.* 30, 1804327.

33. Li, G. (2020) Direct laser writing of graphene electrodes. *J. Appl. Phys.* 127, 010901.

34. Tao, L. -Q. *et al.* (2017) An intelligent artificial throat with sound-sensing ability based on laser induced graphene. *Nat. Commun.* 8, 14579.

35. Duy, L.X. et al. (2018) Laser-induced graphene fibers. *Carbon* 126, 472–479.

36. Wang, L. *et al.* (2020) A comparative study of laser-induced graphene by CO_2 infrared laser and 355 nm ultraviolet (UV) laser. *Micromachines* 11, 1094.

37. Abdulhafez, M. *et al.* (2021) Fluence-dependent morphological transitions in laser-induced graphene electrodes on polyimide substrates for flexible devices. *ACS Appl. Nano Mater.* 4, 2973–2986.

38. Garland, N. T. *et al*. (2018) Flexible laser-induced graphene for nitrogen sensing in soil. *ACS Appl. Mater. Inter*. 10, 39124–39133.

39. Ma, J. *et al.* (2009) Stone-Wales defects in graphene and other planar s p 2-bonded materials. *Phys. Rev. B* 80, 033407.

40. Luong, D. X. *et al.* (2018) Laminated object manufacturing of 3D-printed laser-induced graphene foams. *Adv. Mater.* 30, 1707416.

41. Sha, J. *et al.* (2017) Three-dimensional printed graphene foams. *ACS Nano* 11, 6860–6867.

42. Liu, Y. Q. *et al.* (2016) Surface and interface engineering of graphene oxide films by controllable photoreduction. *Chem. Rec.* 16, 1244–1255.

43. Klemeyer, L. et al. (2021) Geometry-dependent thermal reduction of graphene oxide solid. *ACS Mater. Lett.* 3, 511-515.

44. Cheng, H. *et al.* (2018) Flexible in-plane graphene oxide moisture-electric converter for touchless interactive panel. *Nano Energy* 45, 37–43.

45. Ma, B. *et al.* (2019) The correlation between electrical conductivity and second-order Raman modes of laser-reduced graphene oxide. *Phys. Chem. Chem. Phys.* 21, 10125–10134.

46. Guo, L. *et al.* (2012) Two-beam-laser interference mediated reduction, patterning and nanostructuring of graphene oxide for the production of a flexible humidity sensing device. *Carbon* 50, 1667–1673.47.

47. Jiang, H. B. *et al.* (2014) Bioinspired fabrication of superhydrophobic graphene films by two-beam laser interference. *Adv. Funct. Mater.* 24, 4595–4602.

48. Wang, Z. L. *et al.* (2015) Progress in triboelectric nanogenerators as a new energy technology and self-powered sensors. *Energy Environ. Sci.* 8, 2250–2282.

49. Zou, Y. *et al.* (2020) Wearable triboelectric nanogenerators for biomechanical energy harvesting. *Nano Energy* 77, 105303.

50. Jiang, C. *et al.* (2019) A multifunctional and highly flexible triboelectric nanogenerator based on MXene-enabled porous film integrated with laser-induced graphene electrode. *Nano Energy* 66, 104121.

51. Zhao, P. *et al.* (2020) Replacing the metal electrodes in triboelectric nanogenerators: High-performance laser-induced graphene electrodes. *Nano Energy* 75, 104958.

52. Konios, D. *et al.* (2015) Reduced graphene oxide micromesh electrodes for large area, flexible, organic photovoltaic devices. *Adv. Funct. Mater.* 25, 2213–2221.

53. Kong, X. *et al.* (2020) Laser-scribed N-doped graphene for integrated flexible enzymatic biofuel cells. *ACS Sustain. Chem. Eng.* 8, 12437–12442.

54. Lee, J. S. *et al.* (2011) Metal–air batteries with high energy density: Li–air versus Zn–air. *Adv. Energy Mater.* 1, 34–50.

55. Wang, M. -Q. *et al.* (2018) Synthesis of M (Fe_3C, Co, Ni)-porous carbon frameworks as high-efficient ORR catalysts. *Energy Storage Mater.* 11, 112–117.

56. Ren, M. *et al.* (2019) Laser-induced graphene hybrid catalysts for rechargeable Zn-air batteries. *ACS Appl. Energy Mater.* 2, 1460–1468.

57. Zhang, F. *et al.* (2018) Highly doped 3D graphene Na-ion battery anode by laser scribing polyimide films in nitrogen ambient. *Adv. Energy Mater.* 8, 1800353.

58. Yi, J. *et al.* (2019) Facile Patterning of Laser-Induced Graphene with Tailored Li Nucleation Kinetics for Stable Lithium-Metal Batteries. *Adv. Energy Mater.* 9, 1901796.

59. Wang, Y. *et al.* (2009) Supercapacitor Devices Based on Graphene Materials. *J. Phys. Chem. C* 113, 13103–13107.

60. Gao, W. *et al.* (2011) Direct laser writing of micro-supercapacitors on hydrated graphite oxide films. *Nat. Nanotech.* 6, 496–500.

61. El-Kady, M. F. *et al.* (2012) Laser scribing of high-performance and flexible graphene-based electrochemical capacitors. *Science* 335, 1326–1330.

62. Song, W. *et al.* (2018) Flexible, stretchable, and transparent planar microsupercapacitors based on 3D porous laser-induced graphene. *Small* 14, 1702249.

63. Rahimi, R. *et al.* (2015) Highly stretchable and sensitive unidirectional strain sensor via laser carbonization. *ACS Appl. Mater. Inter.* 7, 4463–4470.

64. Yang, W. *et al.* (2019) Fabrication of smart components by 3D printing and laser-scribing technologies. *ACS Appl. Mater. Inter.*12, 3928–3935.

65. Bobinger, M. R. *et al.* (2019) Flexible and robust laser-induced graphene heaters photothermally scribed on bare polyimide substrates. *Carbon* 144, 116–126.

66. Toda, K. *et al.* (2015) Recent progress in applications of graphene oxide for gas sensing: A review. *Anal. Chim. Acta* 878, 43–53.

67. Strong, V. *et al.* (2012) Patterning and electronic tuning of laser scribed graphene for flexible all-carbon devices. *ACS Nano* 6, 1395–1403.

68. Zhu, J. *et al.* (2019) Biomimetic turbinate-like artificial nose for hydrogen detection based on 3D porous laser-induced graphene. *ACS Appl. Mater. Inter.* 11, 24386–24394.

69. Lan, L. *et al.* (2020) One-step and large-scale fabrication of flexible and wearable humidity sensor based on laser-induced graphene for real-time tracking of plant transpiration at bio-interface. *Biosens. Bioelectron.* 165, 112360.

70. Xu, C. *et al.* (2020) Skin-interfaced sensors in digital medicine: from materials to applications. *Matter* 2, 1414–1445.

71. Chhetry, A. *et al.* (2020) Black phosphorus@laser-engraved graphene heterostructure-based temperature–strain hybridized sensor for electronic-skin applications. *Adv. Funct. Mater.* 31, 2007661.

72. Rahimi, R. *et al.* (2016) Direct laser writing of porous-carbon/silver nanocomposite for flexible electronics. *ACS Appl. Mater. Inter*. 8 (26), 16907–16913.

73. Xu, Y. *et al.* (2020) Multiscale porous elastomer substrates for multifunctional on-skin electronics with passive-cooling capabilities. *Proc. Natl. Acad. Sci. U. S. A.* 117, 205–213.

74. Xu, G. *et al.* (2018) Detection of neurotransmitters by three-dimensional laser-scribed graphene grass electrodes. *ACS Appl. Mater. Inter*. 10, 42136–42145.

75. Han, T. *et al.* (2019) Multifunctional flexible sensor based on laser-induced graphene. *Sensors* 19 (16), 3477.

76. Sharma, S. *et al.* (2020) Laser induced flexible graphene electrodes for electrochemical sensing of hydrazine. *Mater. Lett.* 262, 127150.

77. Nayak, P. *et al.* (2016) Highly efficient laser scribed graphene electrodes for on-chip electrochemical sensing applications. *Adv. Electron. Mater.* 2, 1600185.

78. Aparicio-Martínez, E. *et al.* (2019) Flexible electrochemical sensor based on laser scribed graphene/Ag nanoparticles for non-enzymatic hydrogen peroxide detection. *Sens. Actuators B Chem.* 301, 127101.

79. Xuan, X. *et al.* (2018) A highly stretchable and conductive 3D porous graphene metal nanocomposite based electrochemical-physiological hybrid biosensor. *Biosens. Bioelectron.* 120, 160–167.

80. Yu, Y. *et al.* (2018) Laser-induced carbon-based smart flexible sensor array for multiflavors detection. *ACS Appl. Mater. Inter*. 10, 34005–34012.

81. Rahimi, R. *et al.* (2017) Highly stretchable potentiometric pH sensor fabricated via laser carbonization and machining of carbon–polyaniline composite. *ACS Appl. Mater. Inter*. 9, 9015–9023.

82. Kucherenko, I. S. *et al.* (2020) Ion-selective sensors based on laser-induced graphene for evaluating human hydration levels using urine samples. *Adv. Mater. Technol.* 5, 1901037.

83. Lin, X. *et al.* (2018) Laser engraved nitrogen-doped graphene sensor for the simultaneous determination of Cd (II) and Pb (II). *J. Electroanal. Chem.* 828, 41–49.

84. Tu, J. *et al.* (2020) The Era of Digital Health: A Review of Portable and Wearable Affinity Biosensors. *Adv. Funct. Mater.* 30, 1906713.

85. Soares, R. R. *et al*. (2020) Laser-induced Graphene electrochemical Immunosensors for rapid and label-free monitoring of Salmonella enterica in chicken broth. *ACS Sens.* 5, 1900–1911.

86. Marques, A. C. *et al*. (2020) Laser-induced graphene-based platforms for dual biorecognition of molecules. *ACS Appl. Nano Mater.* 3, 2795–2803.

87. Fenzl, C. *et al*. (2017) Laser-scribed graphene electrodes for aptamer-based biosensing. *ACS Sens.* 2 (5), 616–620.

88. Tehrani, F. *et al.* (2019) Laser-induced graphene composites for printed, stretchable, and wearable electronics. *Adv. Mater. Technol.* 4, 1900162.

89. Gao, W. *et al.* (2016) Fully integrated wearable sensor arrays for multiplexed in situ perspiration analysis. *Nature* 529, 509–514.

90. Yang, Y. and Gao, W. (2019) Wearable and flexible electronics for continuous molecular monitoring. *Chem. Soc. Rev.* 48, 1465–1491.

91. Bhaumik, A. *et al.* (2017) Reduced graphene oxide thin films with very large charge carrier mobility using pulsed laser deposition. *J. Mater. Sci. Eng.* 6, 1000364.

92. Ye, R. et al. (2017) Laser-induced graphene formation on wood. *Adv. Mater.* 29, 1702211.

93. Zhu, C. et al. (2019) Direct laser writing of graphene films from a polyether ether ketone precursor. *J. Mater. Sci.* 54, 4192–4201.